In Situ Fiber Composites Based on Metallocene Polyethylene Matrices

Miguel Angel Cárdenas,[1,2] Rosestela Perera,[3] Norky Villarreal,[1] Carmen Rosales,[3] José María Pastor[1,2]

[1]*CIDAUT, Research and Development Center in Transport and Energy, Parque Tecnológico de Boecillo 47151, Boecillo, Valladolid, Spain*
[2]*Departamento de Física de la Materia Condensada, E.T.S.I.I. Universidad de Valladolid, Paseo del Cauce s/n 47011, Valladolid, Spain*
[3]*Departamento de Mecánica, Universidad Simón Bolívar, Apdo 89000, Caracas, 1081, Venezuela*

Received 7 February 2007; accepted 20 May 2007
DOI 10.1002/app.26927
Published online 25 July 2007 in Wiley InterScience (www.interscience.wiley.com).

ABSTRACT: Binary blends of metallocene polyethylenes with polyethylenes and polypropylene were made in a corotating twin-screw extruder. A stretching process was carried out afterwards in the melt state at the extruder's exit to study the effect of the induced orientation on their thermal and tensile properties. Capillary rheometry was performed to the neat polymers to determine the viscosity ratios of the blend components as a function of the shear rate. SEM and Micro-Raman analyses were done to study the morphology of the stretched and nonstretched blends. As expected, an increase in the modulus and tensile stress was obtained through blending. Additionally, the elastomeric behavior of the metallocene polyethylene (mPE) sample is observed in all blends and it was not lost through blending. Nevertheless, all blends without stretching exhibited a negative deviation of the linear additivity rule of blending. The stretching of the blends made with metallocene polyethylenes as matrices and other types of PEs as dispersed phase did not improve the tensile properties, although some differences in the dispersed phases were found by DSC, and microfibrils could be seen in the drawn mPE/HDPE blend. However, blending with PP produced an improvement in the modulus and tensile stress of the drawn samples in comparison to their undrawn counterpart. The tensile stresses of PP blends are more sensitive to the drawing process than the modulus, which can be attributed to the appearance of large fibril fractions during this process. J Appl Polym Sci 106: 2298–2312, 2007

Key words: crystallization; *in situ* fiber; metallocene blends; polyolefins; Raman spectroscopy

INTRODUCTION

Fiber-reinforced composites have been extensively studied because of the benefits of their remarkably high stiffness and strength.[1] However, *in situ* organic composite materials have gained considerable interest due to the improved tensile properties and solvent permeability. This consists in dispersing a small proportion of another elongated polymer into a thermoplastic matrix where the orientation is retained by ulterior processing.[2–5]

In situ reinforced composites have many advantages over conventional glass fiber reinforced composites, such as lower energy consumption in melt blending, less machine abrasion, etc.[6–9] On the other hand, efforts to develop polyolefins-based blends have been intensively investigated, as a result of their availability and the favorable combination of the individual properties of the blend components.[10–12] In immiscible polymer blends, their properties greatly depend on the blend morphology, which is basically determined by the following factors: blend composition, interface interaction, viscosity ratio, and melt elasticity of the components and processing conditions.[13,14] Blends of metallocene polyethylenes with conventional polyolefins have also been studied.[15–25] However, very little is known regarding the *in situ* reinforced composites of metallocene polyethylenes with conventional polyolefins.

In the present work, two metallocene polyethylenes of different molecular weights were extruded with another metallocene polyethylene and three conventional polyolefins (high-density polyethylene, linear low-density polyethylene, and polypropylene) as dispersed phases through a circular die and the melts were drawn to produce strands with unidirectional orientation of the dispersed phases. These strands were subsequently pelletized and compression-molded at temperatures below the melting point of the different dispersed polymers to preserve the generated structure. The thermal and tensile properties of the blends without stretching and drawn were studied. Also, the isotropic characteris-

Correspondence to: J. M. Pastor (jmpastor@fmc.uva.es).
Contract grant sponsor: CYTED.

TABLE I
Technical Specifications and Properties of the Neat Polymers

Polymer	Comonomer content (wt %)	Density (g/cm^3)	M_w/M_n	MFI (dg/min)	T_m (°C)
mPE1	33	0.880	54,900/25300	18.0	72
mPE2	40	0.870	51,900/22300	30.0	60
mPE3	16	0.913	45,740/23260	30.0	107
HDPE	–	0.957	161,000/24,400	6.5	128
LLDPE	–	0.931	78,700/18,200	4.6	120
PP	–	0.905	273,200/72,940	10.5	163

tics of the stretched blends were studied by micro-Raman confocal imaging spectroscopy for the blends with PP as the dispersed phase.

EXPERIMENTAL

Materials

Three commercial polyethylenes, Engage 8411 (mPE1), Engage 8400 (mPE2), and Engage 8403 (mPE3), were used. These ethylene/1-octene copolymers were manufactured by DuPont Dow Elastomers and are based on their proprietary metallocene technology. A high-density polyethylene (HDPE) and a linear low-density polyethylene (LLDPE) synthesized with Ziegler-Natta catalysts manufactured by Poliolefinas Industriales C.A. and Resinas Lineales Resilin C.A., respectively, were also employed. The polypropylene (PP) used was Stamylan P 17M10, obtained from DSM. Some technical specifications and properties of the neat polymers are listed in Table I.

Processing

Binary blends (80/20 wt %) of the polyolefins were prepared in a Berstorff ECS(2E25) co-rotating twin-screw extruder ($L/D = 30$ and a diameter of cylinder of 25 mm) at 100 rpm and 0.75 kg/h of mass flow rate. The compositions of the blends are presented in Table II. A stretching process was carried out in the melt state (at the extruder's exit) in each one of the blends with the purpose of studying the effect of inducing an orientation during the cooling (crystallization) on their thermal and tensile properties. The extrudate was drawn by a take-up device located at 2.7 m from the die exit. The take-up speed was set at about 25 cm/s. The draw ratio was defined as the ratio of the linear velocity of the take-up device (V_d) to the linear velocity of the extrudate (V_e):

$$\lambda = V_d/V_e \tag{1}$$

From a deformation point of view, it is more relevant to define an elongational or extensional rate. Then, an apparent elongational rate (ε_e) can be defined as:

$$\varepsilon_e = (V_d - V_e)/\Delta l \tag{2}$$

where Δl is the length between the die and the take-up device. A draw ratio of 2.9 and an apparent extensional rate of 0.6 were used. The cooling of the blend to room temperature was carried out in air during the stretching (Fig. 1). Then, the filament was chopped into pellets. Granules of the blends were compression-molded using a Schwabenthan Polystat 200T hydraulic press at temperatures lower than those needed for the melting of the dispersed phase in order to minimize its deterioration (the dispersed phase should have had by then fibrillar structures). Material samples without stretching (NS) and stretched (S) were studied for comparison purposes. The temperatures of the extruder die and those set for the compression molding process are listed in Table II.

TABLE II
Composition of the Blends, Melting Zone and Die Temperatures, Estimated Temperatures (T_R) of the strand at 25 cm from the die and compression-molding temperatures

Blend	Composition of blends 80/20 (wt %)	Melting zone temperature (°C)	Die temperature (°C)	T_R at 25 cm from the die (°C)	Compression molding temperature (°C)
B1	mPE1/mPE3	150	105	94	90
B2	mPE2/mPE3	150	105	94	90
B3	mPE1/HDPE	180	140	121	110
B4	mPE1/LLDPE	160	115	104	100
B5	mPE1/PP	185	155	134	140
B6	mPE2/PP	185	155	134	140

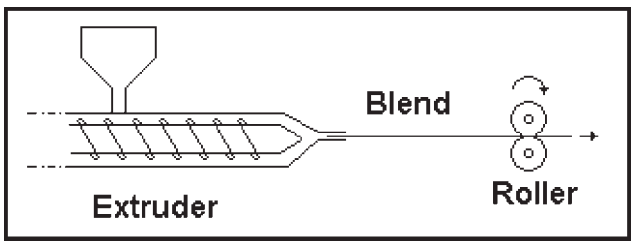

Figure 1 Extruder – Stretching system used to stretch the dispersed phase.

Characterization

The viscosities of the neat components were obtained using a Göttfert Rheograph 2000 capillary rheometer at 150 and 200°C with a capillary die of 1 mm in diameter and L/D ratio of 30/1. These temperatures were selected according to the melt temperatures of the neat polymers and to the different blend compositions, thus the polymers used in PP-based blends were evaluated at 200°C. The viscosity ratios of the polymers subject to blending were determined from the viscosity of the dispersed phase (η_d) and the viscosity of the matrix (η_m) for each blend component in a wide range of shear rates. Tensile tests were performed using a Minimat Polymer Laboratories Tensile tester at a cross-speed of 10 mm/min at room temperature on compression-molded specimens.

The specimens were cryogenically fractured and analyzed by SEM after a process of gold coating. A Jeol-820 scanning electron microscope was used at an accelerating voltage of 15 kV. The dispersed phase domains were observed in the inner zones of the cryogenically fractured tensile specimens. Thermal properties of the materials were determined using a Mettler Toledo DSC 821/400. The scans were performed on small discs of about 10 mg of sample under a nitrogen atmosphere, at 10°C/min as heating and cooling rates. The temperature range scanned went from –80 to 200°C, and backwards. The first and second heatings and first cooling were recorded. The heats of crystallization for 100% crystalline materials were taken as 293 J/g and 207 J/g for PEs and iPP, respectively.[26]

Micro-Raman confocal Labram device from Dilor S. A. was used for Raman confocal measurements. This device uses a He-Ne Laser beam operating at 632 nm, which delivers *ca.* 16 mw at the sample surface. The scattered light is detected with a CCD camera. The spectral resolution was 4 cm^{-1}. Also, neat PP and its blends were cold-drawn with a Minimat tensile equipment at 1 mm/min of cross-speed and micro-Raman confocal measurements were taken in these materials.

RESULTS AND DISCUSSION

Capillary rheometry

Capillary rheometry was employed to characterize the neat polymers under conditions relevant to the subsequent processing. The viscosity curves as a function of the shear rate at 150 and 200°C of the neat polymers are presented in Figures 2 and 3. The viscosities of the polymers decreased as the shear rate increased, indicating a pseudoplastic behavior. The lower shear-thinning character and viscosity values of the mPEs were in agreement with their molecular characteristics (molecular weights and narrow molecular weight distributions). The metallocene-based catalysts produce polyethylenes with a more even distribution of chain branching along the chains and a narrower molecular weight distribution than the Ziegler-Natta catalytic processes do.[19–21]

The viscosity ratios (η_d/η_m) of the binary blend components as a function of shear rate are shown in

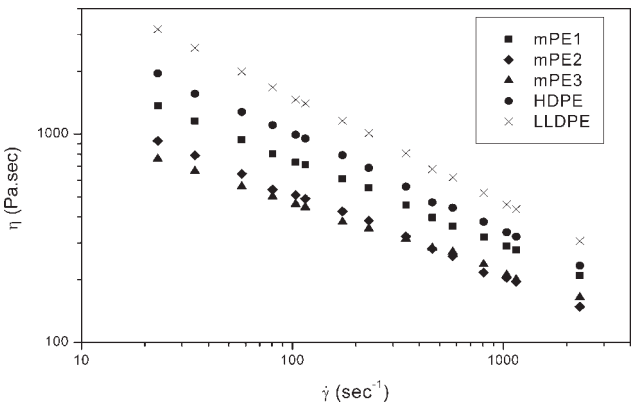

Figure 2 Viscosity as a function of the shear rate of the neat polymers at 150°C.

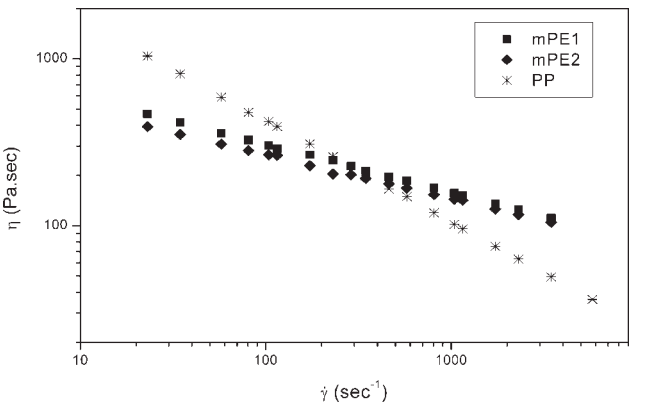

Figure 3 Viscosity as a function of the shear rate of the neat polymers at 200°C.

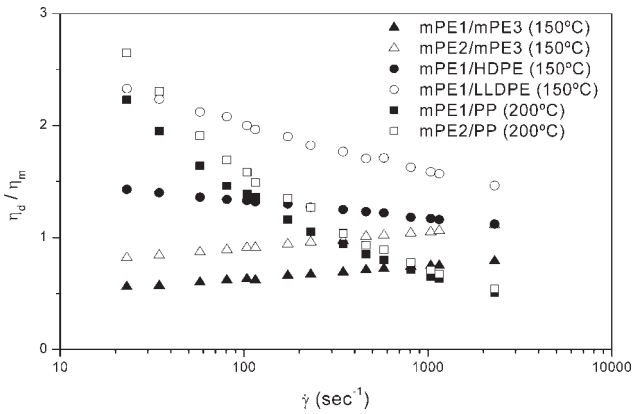

Figure 4 Viscosity ratio of blend components ($p = \eta_d/\eta_m$) as a function of shear rate.

Figure 4. When PP was used as the dispersed phase, the viscosity ratios of the blend components are higher than one and decreased with the increasing shear rate due to the higher shear-thinning behavior of the PP than that of the mPEs materials. The highest viscosity ratio was obtained for the mPE1/LLDPE blend.

SEM morphology

SEM microphotographs of cryogenically fractured surfaces of compression-molded samples and stretched materials (where breakup and coalescence of the dispersed phases could be balanced) of the mPE1/HDPE, mPE1/PP, and mPE2/PP blends are shown in Figures 5–7. These blends were considered the most representative and interesting to study the morphology before and after the stretching process due to the mPE1/HDPE showed an intermediate viscosity ratio curve compared with the other blends. Moreover, the mPE1/PP and mPE2/PP blends were selected to study the effect of the kind of metallocene polyethylene matrix.

The SEM microphotographs of mPE1/HDPE non stretching blend [Fig. 5(a,b)] show a homogeneous and well-dispersed HDPE component within the continuous mPE1 phase, without the presence of voids (homogeneous morphology). This result could be due to the high compatibility in the melt state of mPE1 and HDPE, because of their similar chemical structures and low interfacial tension. On the other hand, the mPE1/PP and mPE2/PP nonstretching blends exhibited many voids (Figs. 6 and 7) from which the dispersed phase could be pulled out (lack of interfacial adhesion). These are typical morphologies of incompatible blends.

The SEM microphotographs of the drawn blends (B3-S, B5-S, and B6-S) are presented in Figures 5(c,d), 6(c,d), 7(c,d). In these microphotographs, elongated particles of the dispersed phase can be seen. The globular particles of the dispersed phases, formed upon extrusion, are mechanically stretched into dispersed phase microfibrils. These microfibrils are embedded into the continuous matrix that could also be oriented. Although the globular particles of PP in mPE1/PP [Fig 6(a,b)] seem smaller than in mPE2/PP [Fig. 7(a,b)], the effectiveness of the stretching process was higher in the mPE2/PP blend than in the mPE1/PP sample, which is evident through the lowest dimension of the elongated particles in these blends [Figs. 6(c,d), 7(c,d)]. In fact, it is well known that it is more difficult to deform a small particle than a larger one, as predicted by Taylor' theory.[27]

The particle size distribution of the PP in the mPE1/PP and mPE2/PP non stretching blends is presented in Table III. Although the number-average diameters (D_n) in both blends are not very different, there are some differences in the weight average diameters (D_w) and the D_v (volume-average diameter)/D_n ratios for PP blends. These parameters were calculated from SEM microphotographs by numerical equations and allowed to obtain quantitative evidences to confirm that the morphology achieved for the PP depends on the metallocene polyethylene matrix. Rana et al.,[15] observed very low interfacial tension between metallocene polyethylene with high comonomer content and PP, which indicated submicron dispersions. This behavior is also observed in this work and explains the differences between the particle sizes of both studied PP blends. Thus, the mPE2 with the higher comonomer content (40 wt %) seemed to have a low interfacial tension with the PP and a broad particle size distribution was obtained. However, these heterogeneous and slightly higher particle sizes have allowed to obtain fibrils with the lowest dimension as was explained above.

The temperatures of the strand surface of each drawn blend just before the take-up rolls was calculated using the model of Bourne and Elliston.[28] The polyethylene density and thermal parameters were assumed to be constant from the die to the rolls. The temperatures obtained at the strands surface of each drawn blend (T_R) are shown in Table II. These temperatures are higher than the crystallization temperatures of the neat blend components. Then, a competition between orientation and relaxation of the blend chains may therefore be expected. The Tjahjadi et al. calculations were used to estimate the relaxation rate of the drawn chains as a function of time.[29] It was found that this relaxation rate is very low for the blends with viscosity ratios higher than one at the processing conditions used. However, in the drawn blends with viscosity ratios lower than one (B1-S and B2-S) the highest relaxation rate was obtained in 10 s. Then, a fibrillar or lamellar morphology for the drawn mPE1/LLDPE blend (B4-S)

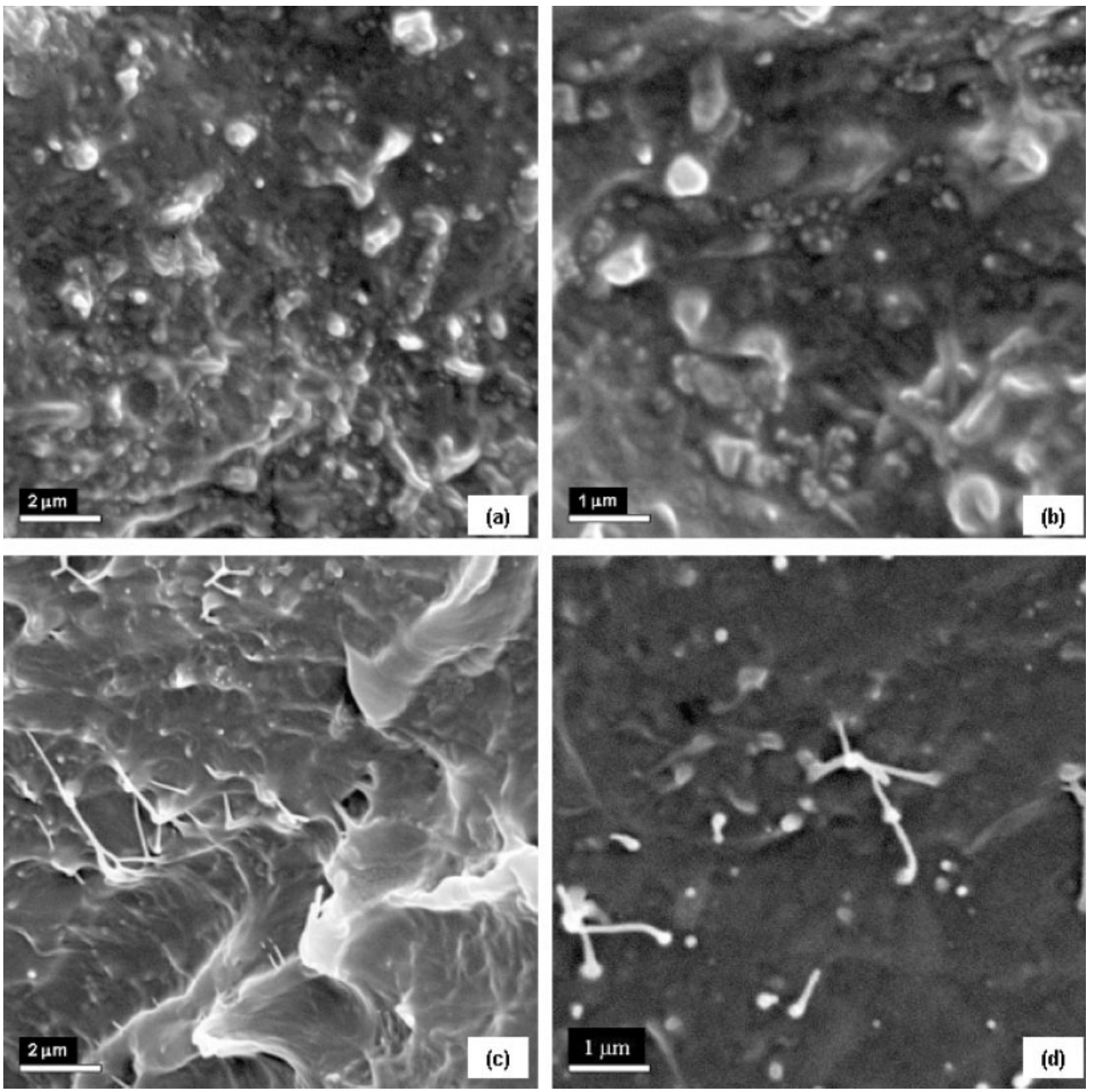

Figure 5 SEM micrographs of cryogenically fracture specimen of mPE1/HDPE blend; (a) and (b): nonstretched blend, and (c) and (d): stretched blend.

could be expected, as was found for B3-S, B5-S, and B6-S, because of the highest viscosity ratio of this likely immiscible blend.

Crystallization behavior

Figures 8–14 show DSC first heating scans for the blends, second heating scans for the neat polymers and first cooling scans of all the materials at 10°C/min. The calorimetric data measured from the DSC thermograms of the neat materials and the melting (T_m) and crystallization (T_c) temperatures of the components of the blends are reported in Tables IV and V, respectively. The broad melting range for the metallocene neat copolymers (mPE1, mPE2, and mPE3) in the second heating (Figs. 8–10) is a consequence of the high comonomer content (1-octene) with a broad crystal size distribution. In some cases, the melting range for copolymers with a very high comonomer content extends to very low temperatures (in the range of −20 to −40°C) and almost overlaps the glass transition temperature.[30] The low values of the

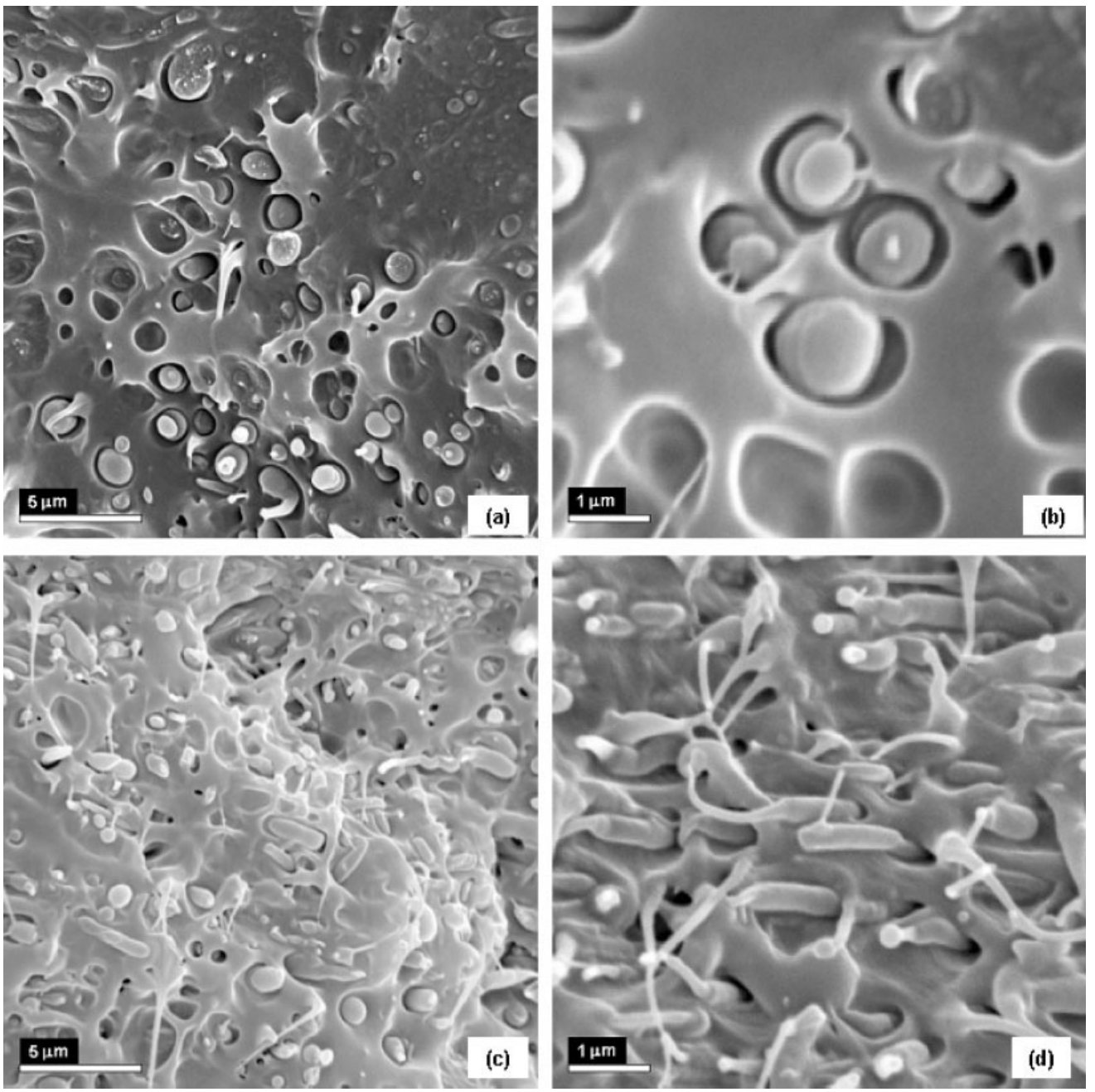

Figure 6 SEM micrographs of cryogenically fracture specimen of mPE1/PP blend; (a) and (b): nonstretched blend, and (c) and (d): stretched blend.

melting enthalpy (ΔH_m) indicate that the metallocene copolymers have also very low degrees of crystallinity (see Table IV) due to the high level of short-chain branching (SCB). As a consequence, mPE2 exhibits a lower value of ΔH_m owing to its higher content of 1-octene. Crystal thickness is also affected by the comonomer content,[31,32] and therefore, the melting and crystallization temperatures (T_m and T_c) for mPE2 are the lowest (Table IV).

Two endotherms could be distinguished in the first heating scans associated to the metallocene copolymers: an intense peak at higher temperatures and a smaller one at about 50°C (not shown here). The first one shifts its position depending on the comonomer content, whereas the second one does not shift considerably. The lower temperature endotherm is associated to the melting of bundled crystals (secondary crystallization) formed by the shorter sequences that were excluded from the primary crystallization (longer crystallizable sequences). In Figure 11 there is evidence of a second crystallization peak at lower temperature in the cooling cycle for the mPE3 material, because of its lower comonomer content (Table I). This peak could indicate phase

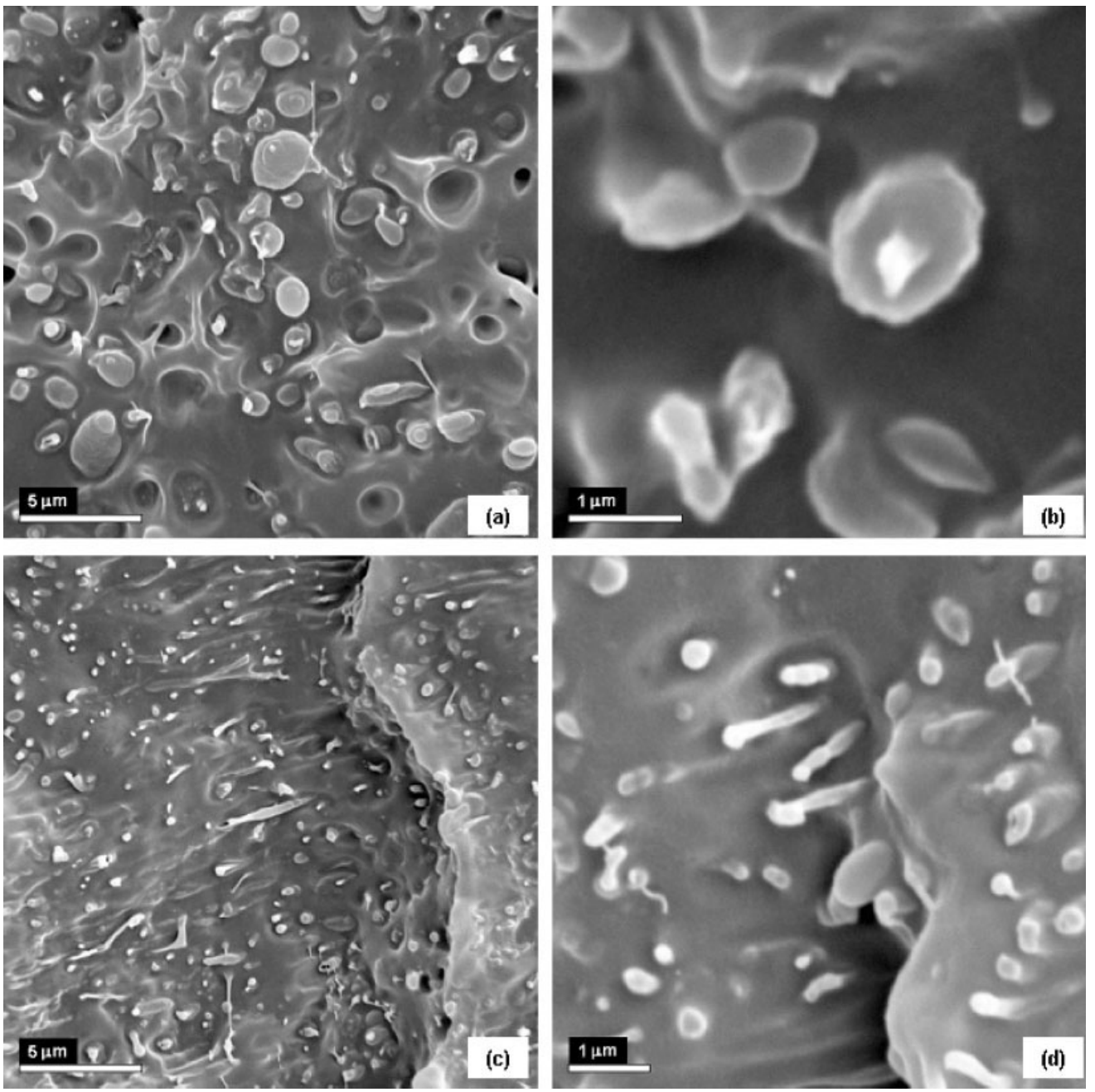

Figure 7 SEM micrographs of cryogenically fracture specimen of mPE2/PP blend; (a) and (b): nonstretched blend, and (c) and (d): stretched blend.

TABLE III
Average Particle Diameters and Number of Particles per cm^3 (Ni)

Blend	D_n (μm)[a]	D_w (μm)[b]	D_v/D_n[c]	Ni × 10^{-11} (cm^{-3})
mPE1/PP	0.7	0.9	2.5	12
mPE2/PP	0.9	1.4	1.7	5

[a] D_n: number-average diameter.
[b] D_w: weight-average diameter.
[c] D_v: volume-average diameter.

separation of low molecular weight material from high molecular weight fractions and/or heterogeneous branching content.[30] The LLDPE and HDPE are ethylene/1-butene copolymers with short chain branching content. Hence, the relatively low crystallinity degree was obtained for this HDPE (Table IV). Finally, iPP displays sharper melting and crystallization peaks characteristics of this polymer (Figs. 10, 13, and 14).[30–33]

All blends exhibited the characteristic behavior of immiscible systems, i.e., the melting endotherms of

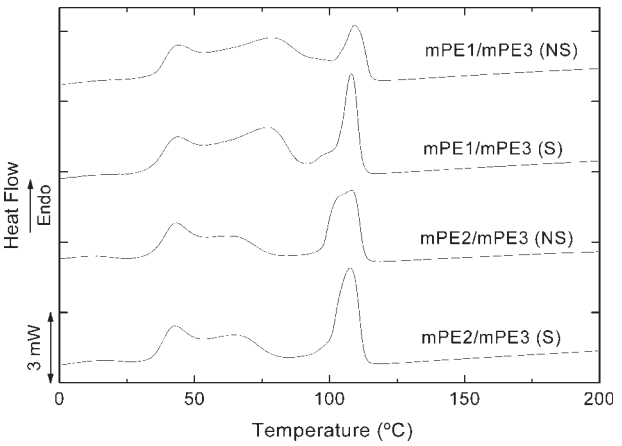

Figure 8 DSC first heating scans of the blends mPE1/mPE3 and mPE2/mPE3.

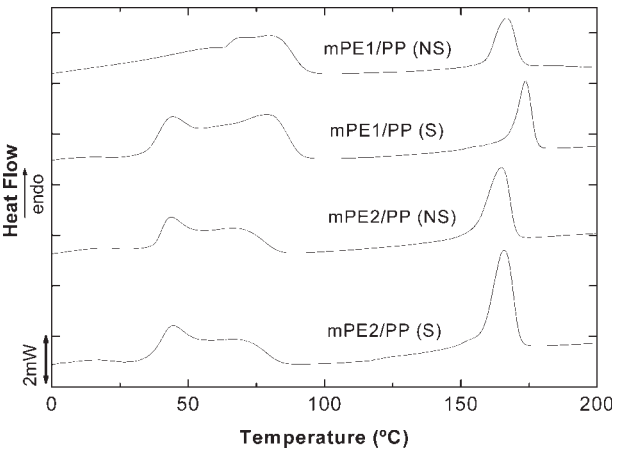

Figure 10 DSC first heating scans of the blends mPE1/PP and mPE2/PP.

both components in the blends were located at about the same temperature range where the neat polymers exhibit their melting transitions in the second heating scan (not shown here). In the mPE1/HDPE, mPE1/PP and mPE2/PP blends, the components showed a clear distinction between the exothermic and endothermic signals of each component without overlapping (see Figs. 9, 10, 13, and 14). As found before by SEM, although there is some compatibility, these blends are immiscible due to the presence of two distinguishable phases. Furthermore, the exothermic signals of the components should be proportional to the blend composition for immiscible blends without interactions. However, the experimental DSC scans of the studied blends exhibited a different and more complex structure. Additionally, the DSC scans of the components are overlapped in the low-temperature regions in the mPE1/mPE3, mPE1/LLDPE, and mPE2/mPE3 blends (Figs. 8, 9, 11, and 12). A correlation between melt compatibilities and tensile properties in LLDPE/HDPE blends was observed by Hussein.[24] However, the miscibility or partial miscibility found in polyethylene blends is very controversial and different behaviors are reported.[10,17–20,33] Several techniques have to be used to study miscibility in PE blends, and only those PE fractions that are similar in chemical structure as regards to content and distribution of short chain branches are probably miscible in the melt.[34,35] In that concern, immiscibility and/or mechanically compatibility was obtained in certain type of blends of mPE/PP.[9,12,15,16,36,37]

Polyethylene blends without stretching

Figures 11 and 12 show the DSC cooling scans of the blends at 10°C/min. The cooling exotherms of the blends without stretching (NS) show two peaks that are located between those two peaks representing the individual neat components. The crystallization exotherms, located at higher temperatures (exotherm

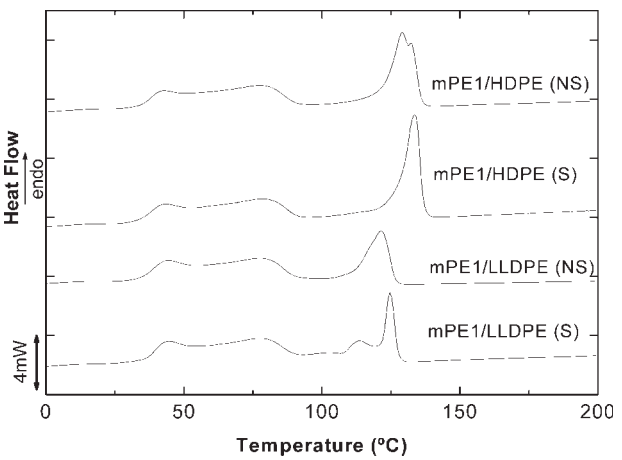

Figure 9 DSC first heating scans of the blends mPE1/HDPE and mPE1/LLDPE.

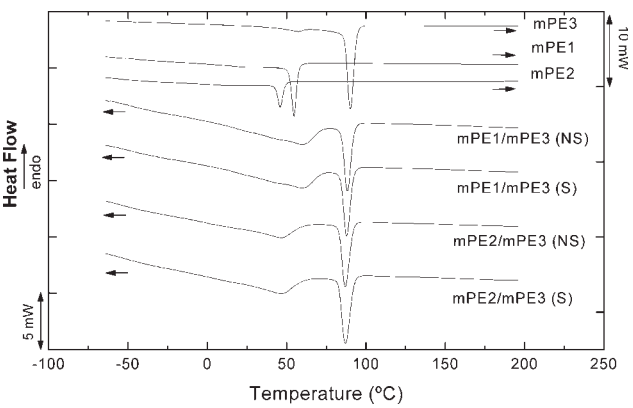

Figure 11 DSC cooling scans of the blends mPE1/mPE2, mPE2/mPE3, and their neat polymers.

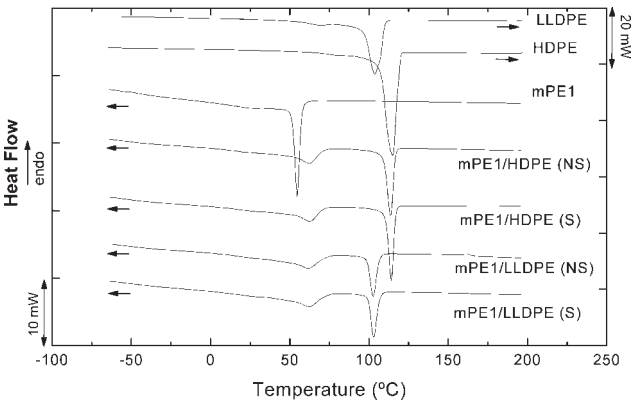

Figure 12 DSC cooling scans of the blends mPE1/HDPE, mPE2/LLDPE, and their neat polymers.

II or T_{c2}), could be attributed to the crystallization of the different dispersed phases used (mPE3, HDPE, and LLDPE), while those at lower temperatures (exotherm I or T_{c1}), could be ascribed to that of the matrix phase, i.e., mPE1 or mPE2. Exotherms II in all polyethylene blends are slightly displaced to lower temperatures as compared to the crystallization of the corresponding neat polymer forming the dispersed phase ($T_{c\text{nm}}$). This fact may be due either to the partial miscibility or to a dilution effect caused by the presence of molten chains of the continuous phases. Therefore, the exotherms I in mPE1/mPE3, mPE1/HDPE, and mPE1/LLDPE blends are displaced to higher temperatures (T_{c1}) when compared to the crystallization of the corresponding matrix phase material. The observed difference could be due to a nucleation effect of the mPE1 rich phase by the dispersed material rich phase (mPE3, HDPE, and LLDPE), as well as to partial miscibility. This partial miscibility could be explained by the existence of some segments of the continuous phase material included within the lamellae of the more linear dispersed phases. The higher crystallization temperature peaks (T_{c2}), and the higher and lower melting temperatures peaks (T_{m2} and T_{m1}) and their depression (ΔT_{c2}, ΔT_{m2}, and ΔT_{m1}) are reported in Tables V and VI. Also, the lower crystallization temperature peaks (T_{c1}) and their enhancements (ΔT_{c1}) are shown in Tables V and VI.

In those blends where there is an overlapping in the DSC exotherm and endotherm signals (mPE1/mPE3, mPE2/mPE3, and mPE1/LLDPE), the height of the temperature peaks in each phase could be proportional to the blend composition if these blends were immiscible without interactions. In all PEs blends, the sharpness of the lower crystallization peak and their heights decrease. However, the height of the high crystallization peak increases for mPE1/mPE3, mPE2/mPE3, and mPE1/LLDPE blends and decreases for the mPE1/HDPE sample. This result could be due to the fact that more linear chains of the continuous phase (mPE1) can be accommodated into the lamellae of the dispersed phase material by decreasing the linear content in the matrix phase. The ratio of the heights of the high and low crystallization peaks of the blends to those of the neat materials ($Y_{c2}/Y_{c2\text{nm}}$ and $Y_{c1}/Y_{c1\text{nm}}$) and the ratio of the heights of the high to the low crystallization peak of the blends (Y_{c2}/Y_{c1}) are reported in Table VI. The height ratios corresponding to the neat materials ($Y_{c2\text{nm}}/Y_{c1\text{nm}}$) and the crystallinity degree of the blends, calculated using an additivity rule of blending, are also presented in Table VI.

On the other hand, the melting endotherms I (T_{m1}) and II (T_{m2}), corresponding to the fusion of the crystals formed in exotherms I and II are displaced to lower temperatures as compared to the endotherms of the neat components for the mPE1/mPE3, mPE1/HDPE, and mPE1/LLDPE blends (see Table V). The

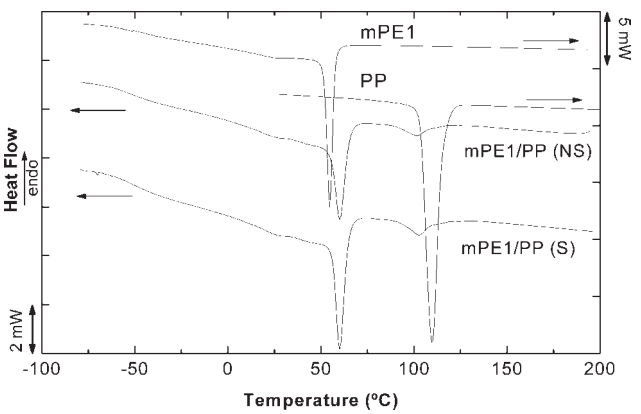

Figure 13 DSC cooling scans of the blend mPE1/PP and its neat polymers with a standard previous heating at 200°C for 5 min.

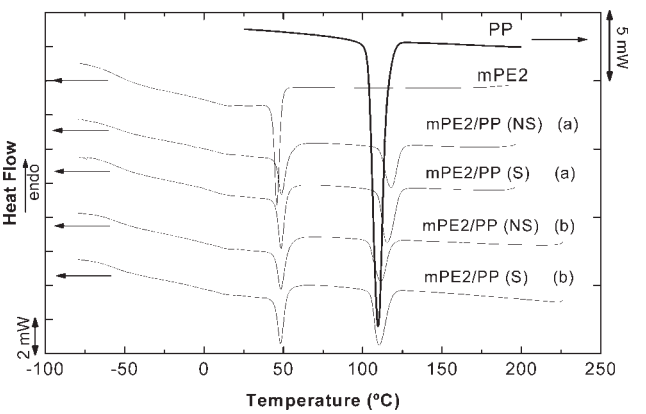

Figure 14 DSC cooling scans of the blend mPE2/PP and its neat polymers with a standard previous heating of: (a) at 200°C and (b) at 230°C for 5 min.

TABLE IV
Thermal Properties of the Neat Polymers

Material	T_m (°C)[a] (±2)	T_c (°C) (±2)	ΔH_m (J/g)[a] (±3)	Crystallinity (%)	Crystallization range (°C)
mPE1	78	55	76	27	−40–67
mPE2	64	46	60	21	−40–72
mPE3	110	91	152	46	−30–97
HDPE	131	116	196	67	60–121
LLDPE	124	104	146	50	30–115
PP	161	106	99	46	90–125
stretched PP	161	112	99	48	90–125

[a] T_m and ΔH_m are the second melting peak temperatures and melting enthalpy, respectively.

melting point depression of the endotherm II could be due to a combination of dilution effects and the formation of co-crystals. The melting temperature of endotherm II in the mPE2/mPE3 blend is lower than that corresponding to mPE3 neat component. Then, mPE3 will crystallize in a melt of mPE2 chains and will melt also in the presence of molten mPE2. This can induce a dilution effect that would depress the melting point of the mPE3 crystal, besides lowering T_c. Therefore, the nucleation effect of the dispersed phase in the continuous phase of the PE blends was not observed because an increase in the crystallization and melting temperatures of the matrix component should be obtained (usually the shift in T_c would be higher than that of T_m). The discrimination between partial miscibility, reorganization during the heating scan and diluting actions in PE blends is not easy based only on the dynamic thermal behavior obtained by DSC. Other effects, such as the kinetic effect of one solid phase which may obstruct or make irregular growth of the lamellar crystallites or the spherulites of the other phase, and thermal perturbations due to different rates of crystallization between the components should be taken into account. However, the results found for the mPE1/mPE3 and mPE1/LLDPE blends may indicate partial miscibility for these blends and interactions between the phases for the other PE blends (mPE2/mPE3 and mPE1/HDPE).[30,33–35] In any case, the presence of two well-defined exotherms indicates that phase separation during crystallization is predominating, even if some interaction between the components is present.

Polypropylene blends without stretching

Figure 10 shows only slight changes in the melting temperature peaks of the components in the melting

TABLE V
Melting and Crystallization Temperatures of the Blend Components[a]

Blend	Condition	T_{m1} (°C)	T_{m2} (°C)	T_{c1} (°C)	T_{c2} (°C)	$T_{conset1}$ (°C)	$T_{conset2}$ (°C)
B1	NS	44–80	109	60	89	74	87
	S	43–78	108	59	88	74	90
B2	NS	43–65	108	46	87	53	101
	S	44–65	108	46	87	57	104
B3	NS	42–79	129–132	62	114	57	148
	S	43–80	133	63	115	59	149
B4	NS	45–79	122	62	103	56	101
	S	44–80	124	62	103	57	99
B5	NS	44–78	167	60	102	70	125
	S	44–80	173	60	103	70	125
B6	NS	43–70	172	49	112	90	125
	S	44–70	166	48	111	90	125

[a] T_{m1} and T_{m2} are the first melting peak temperatures of matrix and dispersed phase, T_{c1} and T_{c2} are the crystallization peak temperatures of matrix and dispersed phase, $T_{conset1}$ and $T_{conset2}$ are the crystallization onset temperatures of matrix and dispersed phase and NS an S are blends without stretching and stretched after the extruder device, respectively.

TABLE VI
Thermal Properties of the PE Blends without Stretching (NS)

Blend/ Property[a]	mPE1/ mPE3 (B1)	mPE2/ mPE3 (B2)	mPE1/ HDPE (B3)	mPE1/ LLDPE (B4)
ΔT_{cnm}	36	45	61	49
ΔT_c	29	42	52	41
ΔT_{c1}	5	0	7	7
ΔT_{c2}	2	3	2	1
ΔT_{m1}	7	0	3	3
ΔT_{m2}	5	5	3	4
Y_{c2nm}/Y_{c1nm}	1.6	3.3	2.6	1.3
Y_{c2}/Y_{c1}	14	13	8	10
Y_{c2}/Y_{cnm}	1.4	1.4	0.7	1.6
Y_{c1}/Y_{cnm}	0.16	0.34	0.21	0.22
Crystallinity (%)	22	20	26	22

[a] The ''nm'' subscript means neat polymers. $\Delta T_{cnm} = T_{c2nm} - T_{c1nm}$ and $\Delta T_c = T_{c2} - T_{c1}$.

process of the blends with PP as the dispersed phase, after being crystallized at 10°C/min of cooling rate. However, the DSC crystallization exotherms are very different for these blends without stretching. In the mPE2/PP blend, a nucleation effect of the mPE2 phase on the PP phase can be observed. The crystallization peak temperature of the PP phase (T_{c2}) is displaced towards higher temperatures (Fig. 14, and Table VII). Therefore, a fractionated crystallization phenomenon was observed for the mPE1/PP blends. A lower temperature crystallization peak and broader exotherm can be observed for the PP phase (Fig. 13). It is well known that, when an immiscible blend component undergoes fractionated crystallization because it is in the form of well-dispersed droplets, the extent of crystallization during cooling from the melt is usually lower than that of the bulk polymer. Hence, the low melting enthalpy obtained for this blend (see Table VII).[12,20] The level of dispersion and the average particle number per cm^3 (Ni) achieved during blending when PP was the dispersed phase are very similar (Table III). However, the fractionated crystallization phenomenon was not observed in the mPE2/PP blend. The heterogeneous nuclei density in iPP reported in the literature is about 9×10^6 nuclei/cm^3, and the density of dispersed droplets (Ni) in these blends met the conditions for fractionated crystallization. Nevertheless, the fractionated crystallization process can be prevented if the matrix can nucleate the dispersed phase, as was observed in the mPE2/PP blend.[36,37] The ratio of the crystallization enthalpies of each component of the blends and the neat components ($\Delta H_{c1}/\Delta H_{c1nm}$ and $\Delta H_{c2}/\Delta H_{c2nm}$) and the crystallinity of the blends with PP are also presented in Table VII.

TABLE VII
Thermal Properties of HDPE and PP Blends without Stretching (NS)

Blend/Property[a]	mPE1/ HDPE (B3)	mPE1/ PP (B5)	mPE2/ PP (B6)
ΔT_{cnm}	61	51	60
ΔT_c	52	42	63
$\Delta T_{c1} = T_{c1} - T_{c1nm}$	7	5	3
$\Delta T_{c2} = T_{c2} - T_{c2nm}$	−2	−4	6
$\Delta T_{m2} = T_{m2} - T_{m2nm}$	−3	5	0
$\Delta H_{c2nm}/\Delta H_{c1nm}$	2.4	1.2	1.6
$\Delta H_{c2}/\Delta H_{c1}$	0.66	0.07	0.29
$\Delta H_{c1}/\Delta H_{c1nm}$	0.70	0.77	0.95
$\Delta H_{c2}/\Delta H_{c2nm}$	0.76	0.04	0.71
Crystallinity (%)	26	18	22

[a] The enthalpy of the blend components has been normalized to their content in the blend.

Stretched blends

The main objective of this work was to show the differences in the end properties of the blends induced by the melt stretching of the dispersed phase (Figs. 8–10). Thus, crystallization differences of the matrix phase within the two conditions (without stretching, NS and stretched, S) are displayed in Tables V and VIII for the mPE1/HDPE, mPE1/PP, and mPE2/PP blends. In most of them, the melting temperatures did not vary with the stretching, but it is seen that the crystallization of the dispersed phases changes during the stretching, and crystals with more uniform thicknesses seems to be produced (see Figs. 12–14). The ratio of the crystallization and melting enthalpies of the stretched and nonstretched blends for the blend components ($\Delta H_{c1S}/\Delta H_{c1NS}$, $\Delta H_{c2S}/\Delta H_{c2NS}$, and $\Delta H_{m2S}/\Delta H_{m2NS}$) and the increase in the degree of crystallinity in the drawn blends is also presented in Table VIII. A slight increase in the degree of crystallinity was obtained only in the mPE1/PP blend.

As far as the matrices are concerned, there are no differences in their thermal properties because they

TABLE VIII
Thermal Properties of the Stretched blends (S)

Blend/Property[a]	mPE1/ HDPE (B3)	mPE1/PP (B5)	mPE1/PP (B6)
$\Delta H_{c1S}/\Delta H_{c1NS}$	1.0	1.2	0.9
$\Delta H_{c2S}/\Delta H_{c2NS}$	1.0	1.3	1.2
$\Delta H_{m2S}/\Delta H_{m2NS}$	1.1	1.3	1.1
$T_{m2S} - T_{m2NS}$	1	6	−6
Increase in crystallinity respect to nonstretched blends (%)	1.0	1.3	1.0

[a] The enthalpy of the blend components has been normalized to their content in the blend.

were all melted during the molding process when the samples were obtained.

The behavior of the first four blends during the controlled crystallization inside the calorimeter and after the first melting up to 200°C, coincides with what it was theoretically expected. First of all, there are no differences between the NS and S conditions, because after the first heating, the effects induced by the stretching process are eliminated or erased. Moreover, it is noticed that the polymers crystallize in a lesser degree than the pure matrices, due to the fact that when they are dispersed into a blend, the crystallization process is hindered and less chains are included into the crystals.

Tensile properties

The stress–strain curves of the neat polymers and the stretched blends are shown in Figure 15. As expected, an increase in the modulus and tensile stress was obtained through blending. Additionally, the elastomeric behavior of the matrices is observed in all blends and it was not lost through blending. Nevertheless, all blends without stretching (NS) exhibited a negative deviation of the linear additivity rule of blending. The increment of the Young's modulus (E) and the stress at 100 and 250% of elongation obtained for the S and NS blends in relation to the mPE1 and mPE2 products are presented in Figures 16 and 17. The highest increase on the E modulus corresponds to the mPE1/HDPE blend (B3), followed by the mPE1/LLDPE sample (B4), because their structures are similar to that of the matrix and their compatibility is higher, which is also in agreement with the thermal results. High compatibility between mPE and HDPE and a low interfacial adhesion between mPE and PP was detected in other research,[10,17,18,21] confirming our results. The higher Young's modulus value of the mPE1/PP than that of mPE2/PP blend without stretching may be explained from the higher molecular weight of the mPE1 matrix (see Table I). Although the viscosity ratios for mPE1/HDPE and mPE1/LLDPE blends at the process condition are the highest (Fig. 4), the similar molecular structure of the components induces a compatibility with a reduction in their surface tension, increasing the interfacial adhesion and

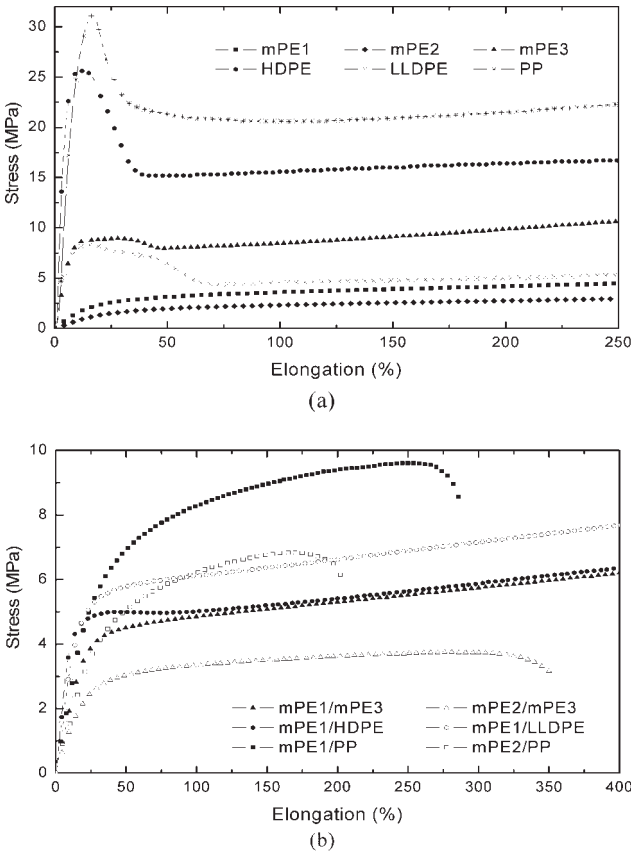

Figure 15 Tensile curves of neat polymers (a) and stretched blends (b).

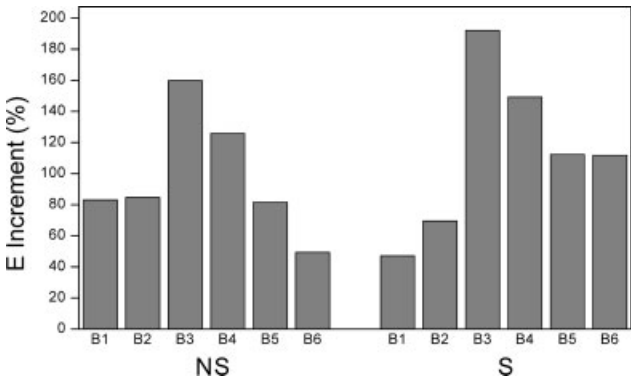

Figure 16 Young's modulus (E) increment (%). B1: mPE1/mPE3, B2: mPE2/mPE3, B3: mPE1/HDPE, B4: mPE1/LLDPE, B5: mPE1/PP, B6: mPE2/PP.

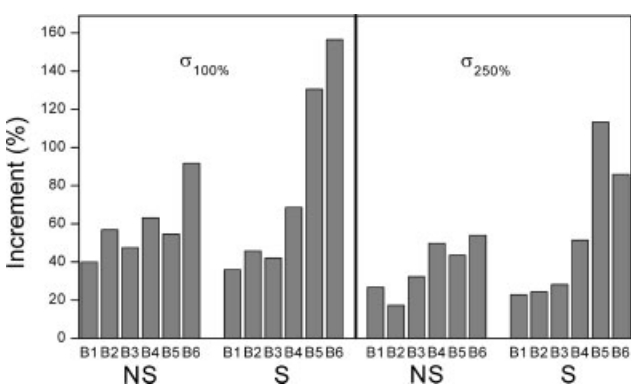

Figure 17 Stress at $\sigma_{100\%}$ and $\sigma_{250\%}$ increment (%) for the two conditions. B1: mPE1/mPE3, B2: mPE2/mPE3, B3: mPE1/HDPE, B4: mPE1/LLDPE, B5: mPE1/PP, B6: mPE2/PP. Stress increment in B6 blend for $\sigma_{250\%}$ corresponds with stress at break (σ_b): 239% for B6 (NS) and 189% for B6 (S).

favouring the fibrillar morphology with an improvement in the mechanical properties. However, the blends with PP as reinforcing phase show lower moduli although this polymer has a high modulus and is easily oriented by stretching. This confirms that the increase in the modulus is dominated by the similarity between the molecular structures, reducing the interfacial tension and leading to a better strain transmission from the matrix to the disperse phase during the melt processing. Partial miscibility or compatibility (very low interfacial tension) between the components of binary blends increased the interfacial adhesion and improved the tensile strength and the elongation at break of the blends.[18,19,24]

The results obtained for the tensile stress at 100 and 250% of elongation (Fig. 17) for the blends without stretching are very different from those of the increment of the Young's modulus. The increase of these values for the mPE1/HDPE and mPE1/LLDPE is smaller than those for the mPE1/PP and mPE2/PP. A small positive deviation of the linear additivity rule of blending in the tensile stresses was obtained for the mPE1/mPE3 and mPE1/LLDPE blends. As it was said before, a possible partial miscibility of these blends was detected through DSC results. On the other hand, a negative deviation of the linear additivity rule of blending for the tensile stresses was found for the other blends.

The stretching of the blends made with metallocene polyethylenes as matrices and other types of PE as dispersed phase (B1-S, B2-S, B3-S, and B4-S) did not improve the tensile properties, although some differences in the dispersed phases were found by DSC and microfibrils could be seen in the drawn mPE1/HDPE blend [Fig. 5(c,d)]. Yet, the overall result is an improvement in the modulus and tensile stress of the drawn samples in comparison to their undrawn counterpart in the PP blends. The tensile stresses of PP blends are more sensitive to the drawing process than the modulus, which can be attributed to the appearance of large fibril fractions when the drawing takes place [Figs. 6(c,d), 7(c,d)]. The similar modulus values of both stretched blends could be explained as a consequence of the interactions between mPE2 and PP, as found by SEM. The tensile strength at 189% of elongation was reported for the mPE2/PP blend because this stretched blend fractured before 250% of elongation. Similar results were obtained in other works with *in situ* fibrillar morphology.[2,3,6,8] An increase of 82 and 54% in the Young's modulus and yield stress values were found for a PE/PA-6 blend with *in situ* fibrillar morphology.[3]

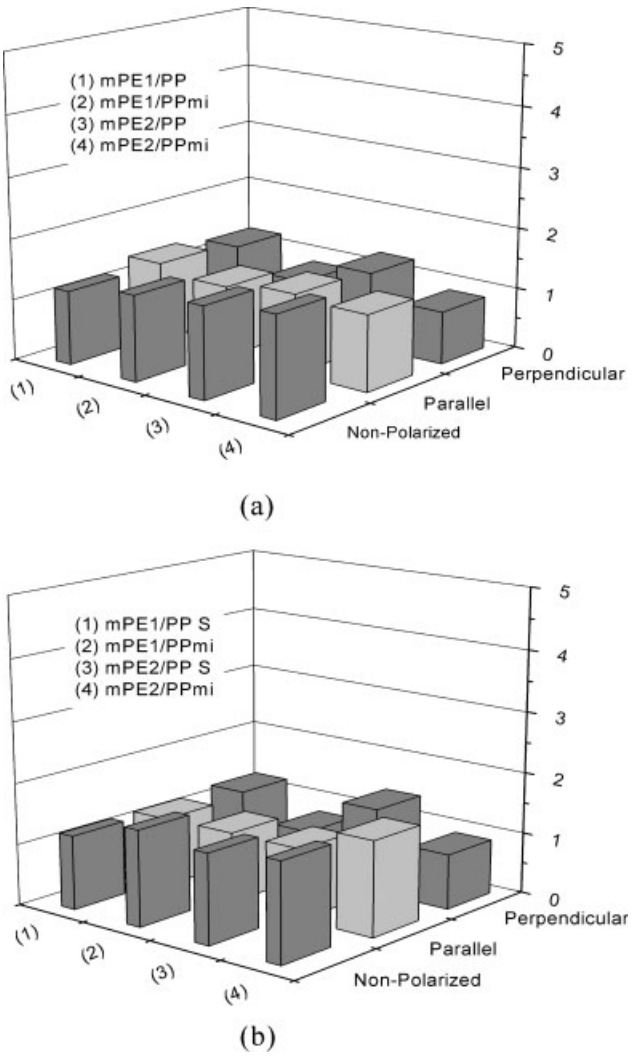

Figure 19 Intensity relation ($I_{1067cm^{-1}}/I_{1132cm^{-1}}$) corresponding to PE bands in the blends (a) Nonstretching condition (NS) and (b) Drawn condition (S).

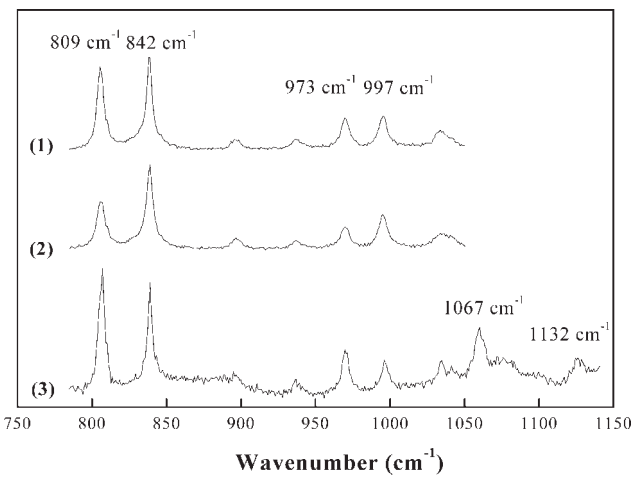

Figure 18 Micro-Raman confocal spectra of (1) neat PP, (2) stretched neat PP (PPmi) and (3) stretched mPE2/PP (S) blend.

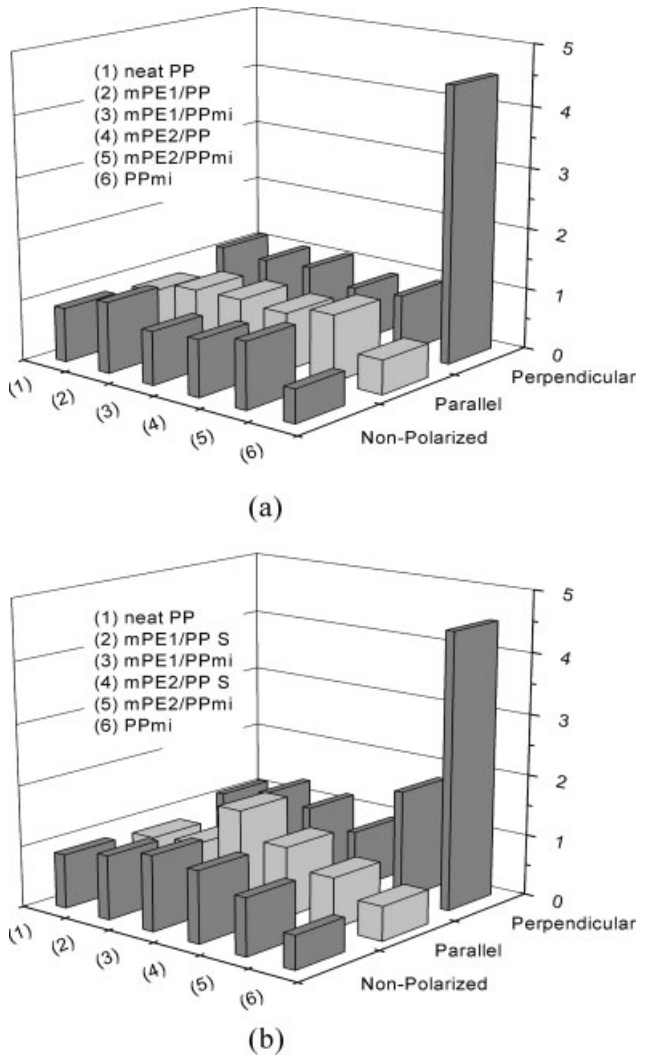

Figure 20 Intensity relation ($I_{809cm^{-1}}/I_{841cm^{-1}}$) corresponding to PP bands in the blends (a) Nonstretching condition (NS) and (b) Drawn condition (S).

Micro-Raman confocal spectroscopy

The mechanical properties, such as tensile strength and Young's modulus of an in-situ fibrillar composite are different in the different directions because the anisotropy of this type of materials. However, when the *in situ* composite is pelletized and a physical preblend is made before compression-molding, a more homogeneous material is expected. To study the anisotropy of the stretched blends with PP as the dispersed phase and the possibility of obtaining an additional orientation by cold-drawing, micro-Raman confocal spectroscopy was performed. The representative Raman spectra of neat and stretched PP and mPE2/PP (B6-S) drawn in a Minimat tensile equipment are presented in Figure 18. For PP, the bands at 809, 842, 973, and 997 cm^{-1} are attributed to chain orientations and in particular, as the degree of crystallinity of the materials rises, the intensity of the band at 842 cm^{-1} rises relative to that at 809 cm^{-1}.[38–40] On the other hand, a comparison of intensities of oppositely polarized PE bands at 1067 and 1132 cm^{-1} allows the possibility of estimating the orientation of PE chains.[41] In Figure 19, the intensity ratios I_{1067}/I_{1132} of blends with PP are presented with nonpolarized laser and polarized, parallel or perpendicular to the stretching direction. Only very small differences between the intensity ratios at opposite orientation of the laser polarization were found. So, no preferred average orientation was obtained for the PE chains in these blends. The intensity ratios I_{809}/I_{841} are minimal if the chains are parallel to the laser polarization and reach maximum values if the chains are perpendicular to the polarization. The intensity ratios I_{809}/I_{842} of neat PP and its blends, as well as the cold-drawn neat PP and its blends with a Minimat tensile equipment are shown in Figure 20. Only very small differences between the intensity ratios at opposite orientation of the laser polarization were obtained for the neat PP and its blends (B5-NS, B5-S, B6-NS, and B6-S). As it could be expected, with the compression-molded blends, no preferred average orientation was found. The formation of an optical anisotropy can be seen for the Raman bands of neat PP only after plastic cold-drawing.[42] Similarly, only after cold-drawing, the usual Raman Spectra manifest an additional uniaxial orientation of PP chains for the B6-S blend

TABLE IX
Values of the Expression $Y = 2(R^{90-} - R^0)/(R^{90} + R^0)$ for the Blends

Property/Blend	Y (1067 cm^{-1}/1132 cm^{-1}) PE bands	Y (809 cm^{-1}/841 cm^{-1}) PP bands
Neat PP	–	0.35 (none or weak orientation)
PP (mi)	–	1.56 (medium orientation)
B5-NS	−0.08	0.08
B5-NS (mi)	−0.32 (PE weak orientation)	0.10
B5-S	0.06	0.32
B5-S (mi)	−0.41 (PE weak orientation)	−0.27
B6-NS	−0.05	−0.03
B6-NS (mi)	−0.37 (PE weak orientation)	−0.14
B6-S	0.19	−0.18
B6-S (mi)	0.53 (PE weak orientation)	0.73 (weak orientation)

drawn with a tensile equipment. To obtain a quantitative estimation of chain orientation in the PE and PP components of the blends where PP is the dispersed phase, the following expression was used:[41]

$$Y = 2(R^{90} - R^0)/(R^{90} + R^0) \quad (3)$$

where the R values are the intensity ratios of the bands I_{1067}/I_{1132} and I_{809}/I_{842} for 0 and 90 degrees of orientation of the samples. The values of this function Y were calculated and are reported in Table IX for the neat PP, the blends with PP without stretching and stretched after extrusion, and the samples drawn in a Minimat tensile equipment (mi). Only a certain orientation in PE chains is observed for the samples drawn in the Minimat tensile equipment. In the PP phase, a weak orientation of the chains is obtained in the B6-S blend drawn in the Minimat and medium and none orientations were found in the neat PP and other blends drawn in the Minimat, respectively. This last result may be an additional evidence of interactions between these blend's components, as it is the fact of tensile stress transfer obtained in this B6-S blend. Similar results for drawn PP were obtained by López et al.[39] Hence, these results confirmed that a totally homogeneous and anisotropic material was obtained after the compression-molding process.

CONCLUSIONS

As expected, an increase in the modulus and tensile stress was obtained through blending. Additionally, the elastomeric behavior of the matrices (mPE1 and mPE2) was observed in all blends and it was not lost through blending. Nevertheless, all blends without stretching exhibited a negative deviation of the linear additivity rule of blending.

The stretching of the blends made with metallocene polyethylenes as matrices and other types of PEs as dispersed phase did not improve the tensile properties, although some differences in the dispersed phases were found by DSC, and microfibrils could be seen in the drawn mPE1/HDPE blend. However, blending with PP produced an improvement in the modulus and tensile stress of the drawn samples in comparison to their undrawn counterpart. The tensile stresses of PP blends are more sensitive to the drawing process than the modulus, which can be attributed to the appearance of large fibril fractions due to the drawing process.

References

1. Lutz, J. T. Thermoplastics Polymer Additives; Marcel Dekker: London, 1989.
2. Faisant, J. B.; Aït-Kadi, A.; Buosmina, M.; Deschenes, L. Polymer 1998, 9, 533.
3. Chen, J. C.; Harrison, R. Polym Eng Sci 1998, 38, 371.
4. Monticciolo, A.; Cassagnau, P.; Michel, A. Polym Eng Sci 1998, 38, 1882.
5. Li, X.; Chen, M.; Huang, Y.; Cong, G. Polym Eng Sci 1999, 39, 881.
6. Liang, Y. C.; Isayev, A. I. Polym Eng Sci 2002, 42, 994.
7. Boyaud, M. F.; Cassagnau, P.; Michel, A.; Bousmina, M.; Aït-Kadi, A. Polym Eng Sci 2001, 41, 684.
8. Evstatiev, M.; Schultz, J. M.; Fakirov, S.; Friedrich, K. Polym Eng Sci 2001, 41, 192.
9. Zhang, L.; Huang, R.; Wang, G.; Li, L.; Ni, H.; Zhang, X. J Appl Polym Sci 2002, 86, 2085.
10. Lee, H. S.; Denn, M. M. Polym Eng Sci 2000, 40, 1132.
11. Kim, B. K.; Do, I. H. J Appl Polym Sci 1996, 60, 2207.
12. Li, J.; Shanks, R. A.; Olley, R. H.; Greenway, G. R. Polymer 2001, 42, 7685.
13. Baker, W.; Scott, C.; Hu, G. H. Reactive Polymer Blending; Hanser: Munich, 2001.
14. Sundararaj, U.; Macosko, C. W. Macromolecules 1995, 28, 2647.
15. Rana, D.; Lee, H.; Cho, K.; Lee, B. H.; Choe, S. J Appl Polym Sci 1998, 69, 2441.
16. Kukaleva, N.; Cser, F.; Jollands, M.; Kosior, E. J Appl Polym Sci 2000, 7, 1591.
17. Kwang, H.; Rana, D.; Cho, K.; Rhee, J.; Woo, T.; Lee, B.; Choe, S. Polym Eng Sci 2000, 40, 1672.
18. Guimaraes, M.; Cotinho, F.; Rocha, M.; Garcia, M. J Appl Polym Sci 2001, 81, 1997.
19. Guimaraes, M.; Cotinho, F.; Rocha, M.; Farra, M.; Bretas, R. J Appl Polym Sci 2002, 86, 2240.
20. Di, Y.; Iannace, S.; Nicolais, L. J Appl Polym Sci 2002, 86, 3430.
21. Liu, C.; Wang, L.; He, J. Polymer 2002, 43, 3811.
22. Peng, Y.; Zhang, Q.; Du, R.; Fu, Q. J Appl Polym Sci 2005, 96, 1816.
23. Fang, Y.; Carreau, P.; Lafleur, P. Polym Eng Sci 2005, 45, 1254.
24. Hussein, I. Polym Inter 2004, 53, 1327.
25. Hussein, I. Polym Int 2005, 54, 1330.
26. Wunderlich, B. Thermal Analysis; Academic Press: London, 1990.
27. Taylor, G. I. Proc R Soc Lond A 1934, 146, 501.
28. Middleman, S. Fundamentals of Polymer Processing; McGraw-Hill: USA, 1977.
29. Tjahjadi, M.; Ottino, J. M.; Stone, H. A. AICHE J 1994, 40, 385.
30. Benedikt, G. M. Metallocene Technology in Commercial Applications; Plastics Design Library (Society of Plastics Engineers): New York, 1999.
31. Benavente, R.; Pérez, E.; Quijada, R. J Polym Sci Part B: Polym Phys 2001, 39, 277.
32. Dias, M. L.; Barbi, V. V.; Pereira, R. A.; Mano, E. B. Mat Res Innov 2001, 4, 82.
33. Puig, C.C. Polym Bull 1997, 38, 715.
34. Arnal, M. L.; Sánchez, J. J.; Müller, A. J. Polymer 2001, 42, 6877.
35. Arnal, M. L.; Cañizalez, E.; Müller, A. J. Polym Eng Sci 2002, 42, 2048.
36. Manaure, A. C.; Morales, R. A.; Sánchez. J. J.; Müller, A. J. J Appl Polym Sci 1997, 66, 2481.
37. Manaure, A. C., Müller, A. J. Macromol Chem Phys 2000, 201, 958.
38. Meier, R. J.; Kip, B. J. Microbeam Analysis; San Francisco Press: USA, 1994.
39. López-Quintana, S.; Schmidt, P.; Dybal, J.; Kractochíl, J.; Pastor, J. M.; Merino, J. C. Polymer 2002, 43, 5187.
40. Arruebarrena de Baéz, M.; Hendra, P. J.; Judkins, M. Spectrochim Acta A 1995, 51, 2117.
41. Lagarón, J. M.; López-Quintana, S.; Rodríguez-Cabello, J. C.; Merino, J. C.; Pastor, J. M. Polymer 2000, 41, 2999.
42. Wang, X.; Michielsen, S. J Appl Polym Sci 2001, 82, 1330.